Journal of Power Sources 226 (2013) 202–209

Contents lists available at SciVerse ScienceDirect

Journal of Power Sources

journal homepage: www.elsevier.com/locate/jpowsour

# The effects of electrolyte on the supercapacitive performance of activated calcium carbide-derived carbon

Hao Wu, Xianyou Wang*, Lanlan Jiang, Chun Wu, Qinglan Zhao, Xue Liu, Ben'an Hu, Lanhua Yi

*Key Laboratory of Environmentally Friendly Chemistry and Applications of Minister of Education, School of Chemistry, Xiangtan University, Hunan, Xiangtan 411105, China*

## HIGHLIGHTS

- Comparable electrochemical behaviors of samples in various aqueous electrolytes.
- Comparisons of ions in various aqueous electrolytes are carried out.
- Sample in 6 M KOH has better capacitive behaviors and higher capacitance.

## ARTICLE INFO

*Article history:*
Received 2 August 2012
Received in revised form
9 October 2012
Accepted 8 November 2012
Available online 15 November 2012

*Keywords:*
Calcium carbide-derived carbon
Activation
Electrolyte
Supercapacitors

## ABSTRACT

Porous calcium carbide-derived carbon (CCDC) has been prepared by one-step route from $CaC_2$ in a freshly prepared chlorine environment at lower temperature, and following activated by $ZnCl_2$ to get activated CCDC. The performances of the supercapacitors based on activated CCDC as electrode active material in aqueous KOH, $K_2SO_4$, KCl and $KNO_3$ electrolytes are studied by cyclic voltammetry, constant current charged/discharged, cyclic life and electrochemical impedance spectroscopy. It has been found that the supercapacitor using 6 M KOH as electrolyte shows an energy density of 8.3 Wh $kg^{-1}$ and a power density of 1992 W $kg^{-1}$ based on the total weight of the electrode active materials with a voltage range 0 V–1 V. Meanwhile, the specific capacitance of the supercapacitor in 6 M KOH electrolyte is 68 F $g^{-1}$ at the scan rate of 1 mV $s^{-1}$ in the voltage range of 0 V–1 V, the charge-transfer resistance is extremely low and the relaxation time is the least of all. The supercapacitor also exhibits a good cycling performance and keeps 95% of initial capacity over 5000 cycles.



## 1. Introduction

As we have seen, the most common electrical energy storage devices are batteries and capacitors. Rechargeable batteries generally provide a high specific energy and a rather low specific power. Usually, capacitors can supply high specific powers, but the amount of energy stored is very low. Supercapacitors (often called electrochemical capacitors or ultra-capacitors) are charge-storage devices that possess excellent reversibility, exhibit ideal high power density and fairly long cycle life [1]. They are applied to various electronic devices, such as power electronics, as well as in hybrid electric vehicles and space flight technology [2]. Recently, many researches on the electrochemical capacitors aim to increase power and energy density as well as lower fabrication costs while using environmental friendly materials, which can be realized by using the larger capacitance materials and/or increasing the cell voltages [3].

The electrochemical behaviors of the supercapacitors are decided not only by the exposed surface area of the carbon electrode, but also by the matching degree between the size of solvated ions in the electrolytes and the pore size distribution of carbon electrode [4,5,6]. A lot of efforts have been done on the compatibility of electrodes with electrolytes. In the literature, [7] electrolyte concentration showed a strong effect on supercapacitor capacitance. For example, if electrolyte concentration is high, ion transport within the electrode layer will be easier, leading to an effective building-up for electric double layer. However, if the electrolyte concentration is too high, the viscosity of solution will increase due to less water hydration, resulting in decreases of ion mobility. The properties of solvents in electrolytes also have great impact on the migration speed and size of the solvated ions. For instance, the radius of solvated ions in aqueous solvents is mostly less than that in organic electrolyte. For this reason, a carbon electrode with a larger number of macropores is preferable in organic solvents [8]. However, despite the remarkable performance of these organic-based nonaqueous electrolytes, they suffer from severe safety hazards. The fabrication costs of capacitors using such electrolytes

* Corresponding author. Tel.: +86 731 58292060; fax: +86 732 58292061.
*E-mail address:* wxianyou@yahoo.com (X. Wang).

0378-7753/$ – see front matter © 2012 Elsevier B.V. All rights reserved.
http://dx.doi.org/10.1016/j.jpowsour.2012.11.014

are also high due to the use of a water-free environment needed to manipulate and assemble. For this reason, many researches have focused on choosing proper positive and negative electrode materials to form a hybrid system in aqueous electrolyte. Therefore, finding an eco-friendly and efficient aqueous electrolyte will be highly significant. Indeed recent studies [9,10,11,12] have shown that symmetrical type carbon/carbon capacitor and asymmetric carbon/$MnO_2$ electrochemical capacitors (based on various porous carbon materials) with different aqueous electrolytes of $K_2SO_4$, KCl, $KNO_3$ and KOH possess excellent electrochemical performance, especially with KOH. However, there have been few reports about the effects of electrolyte on the supercapacitive performance of the activated CCDC.

CCDC produced by halogenation of carbides exhibits a narrow pore size distribution, a tunable pore and microstructure by choosing the appropriate carbide precursor and chlorination temperature. Yushin et al. [13] studied the effect of pore size on hydrogen uptake and heat of adsorption about carbide-derived carbons. The results showed how smaller pores increase both the heat of adsorption and the total volume of adsorbed $H_2$. It has been demonstrated that increasing the average heat of $H_2$ adsorption above 6.6 kJ $mol^{-1}$ substantially enhances $H_2$ uptake at 1 atm (1 atm = 101,325 Pa) and −196 °C. The heats of adsorption up to 11 kJ $mol^{-1}$ exceed values reported for metal–organic framework compounds and carbon nanotubes. Schmirler et al. [14] developed an in-situ thermal activation in $CO_2$ parallel to the carbides chlorination for the preparation of carbide-derived carbons. For this in-situ activation and chlorination of carbides the influence of the processing, the concentration of $CO_2$ and activation time on the pore structure of CDC were studied.

In previous work, our group has carried out a lot of works on CCDC and their supercapacitive behaviors. Dai et al. [15] developed a type of one-step preparation technique for CCDC, which was synthesized from $CaC_2$ in a freshly prepared chlorine environment in the temperature range of 100 °C–600 °C. Zheng et al. [16] prepared CCDC/polyaniline (PANI) composite materials by in-situ chemical oxidation polymerization of an aniline solution containing well-dispersed CCDC, the specific capacitance of CCDC/PANI composite electrode showed as high as 713.4 F $g^{-1}$ measured by cyclic voltammetry at 1 mV $s^{-1}$, but the capacitance retention of coin supercapacitor just remained 80% after 1000 cycles. The activation technology will usually influence specific surface area, microstructure and supercapacitive behaviors of porous carbon material. In order to study the effect of activation technology on the electrochemical performances of supercapacitors using CCDC as electrode active material, we have used $H_3PO_4$, $ZnCl_2$ and KOH as activation agent to activate CCDC and found that $ZnCl_2$ was the best activation agent [17]. In this paper we will investigate further the electrochemical performance of activated CCDC in the different aqueous electrolytes, e.g., 0.5 M $K_2SO_4$, 2 M KCl, 1 M $KNO_3$ and 6 M KOH [9,10,11,12].

## 2. Experimental

### 2.1. Synthesis of activated CCDC

All chemicals were of analytical grade and used without any further purification. The CCDC were prepared as follows: $CaC_2$ powders were placed in a quartz tube furnace then the tube was Ar purged for 30 min and heated to 400 °C. Fresh prepared chlorine gas was directly passed through the tube furnace once reached the desired reaction temperature. After chlorination for 2 h, the furnace was naturally cooled down to room temperature under Ar purge. The resultant product was soaked in HCl solution (3 mol $L^{-1}$) and washed with distilled water to remove further remainder. Acidic product was washed into neutral condition and then dried in desiccators at 80 °C for 12 h to obtain CCDC.

The resultant CCDC sample was soaked in $ZnCl_2$ solution (0.37 mol $L^{-1}$) and stirred in 80 °C for 7 h, then filtrated and dried at 80 °C for 12 h. The filtered product was placed in a quartz tube furnace, and the tube was Ar purged for 30 min, then heated to 600 °C. The product was soaked in diluted hydrochloric acid, heated to 90 °C and stirred for 30 min, then washed with distilled water until the pH of filtrate water became neutral. The filtered product was dried at 80 °C for 12 h [18,19].

### 2.2. Preparation of electrode and button cell supercapacitor assembly

The mass ratio of activated CCDC/acetylene black was 8:1. The powder mixture was mixed with 10 wt% of polyvinylidene fluoride (PVDF) aqueous suspension as a binder to obtain a paste. The paste was then pressed into the steel mesh substrate using a spatula. After drying in vacuum at 110 °C for 12 h, the electrode of steel mesh was pressed at 15 M Pa for 1 min to assure a good electronic contact and form a circular tablet. The geometric surface area of the electrodes was kept to be 1.0 $cm^2$; the electrodes typically had a thickness of about 0.1 mm. Symmetrical button cell supercapacitors were constructed with various electrolytes (0.5 M $K_2SO_4$, 2 M KCl, 1 M $KNO_3$ and 6 M KOH), in which two activated CCDC electrodes were separated by a separator of electrode/separator/electrode order. Then the supercapacitors were sealed with a packing machine.

### 2.3. Characterization of the material

The activated CCDC was characterized by physical $N_2$ adsorption/desorption at 77 K (using an AUTOSORB-1 instrument from Quantachrome). The specific surfaces (SBET) were derived from $N_2$ adsorption isotherms by means of the BET equation. The pore size distributions and medium pore diameter were determined using the BJH. The micropore volume ($V_{micro}$) was obtained by Dubinin–Raduskevich equation and the total volume of porous ($V_{total}$) by Gurvitsch rule at $P/P_0 \approx 0.985$.

### 2.4. Electrochemical measurements

The electrochemical performances of the as-prepared electrode materials were characterized by cyclic voltammetry (CV) between −1 V and 0 V with the different scan rates of 1 mV $s^{-1}$–20 mV $s^{-1}$, galvanostatic charge/discharge tests at various constant current densities with cutoff voltage of 0 V–1 V and electrochemical impedance spectroscopy (EIS) in the frequency range from $10^5$ Hz to $10^{-2}$ Hz with amplitude of 5 mV. The CV, the galvanostatic charge/discharge and EIS measurements were performed by means of electrochemical analyzer systems, CHI660 (CH Instruments, USA). The experiments were carried out using button cell supercapacitors. The cycle life was measured by potentiostat/galvanostat (BTS 6.0, Neware, Guangdong, China) on button cell supercapacitors.

## 3. Results and discussion

Cyclic voltammetries are performed to estimate the electrochemical properties of the symmetric supercapacitors with activated CCDC as electrode active materials at the scan rate range of 1 mV $s^{-1}$–20 mV $s^{-1}$ with the voltage range of 0 V–1 V in various aqueous electrolyte solutions. Fig. 1 shows cyclic voltammograms of activated CCDC supercapacitors in the aqueous electrolytes of 6 M KOH, 1 M $KNO_3$, 0.5 M $K_2SO_4$ and 2 M KCl. It can be found from

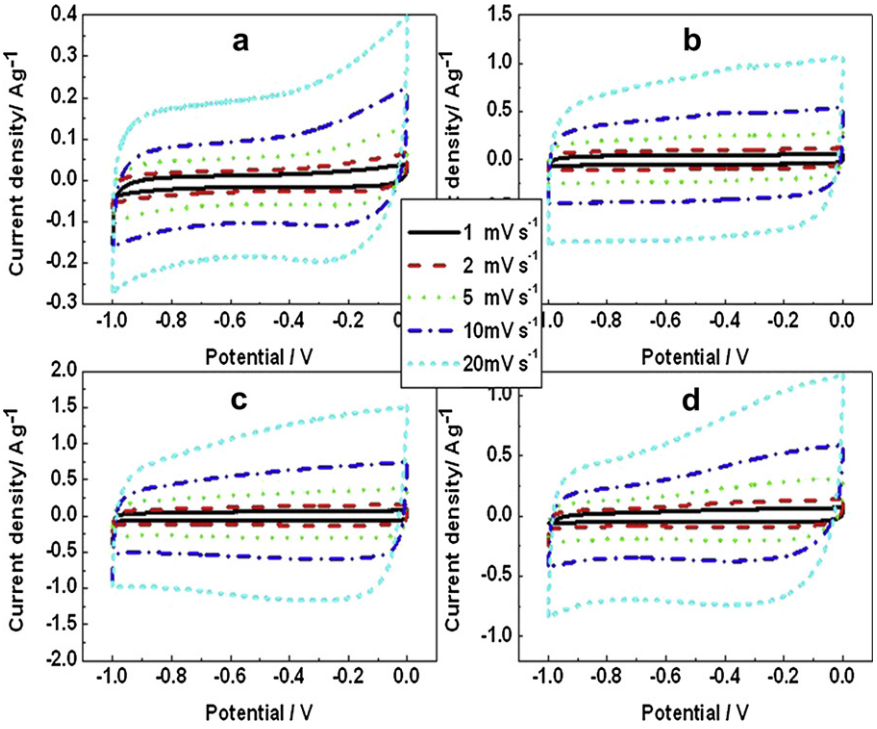


**Fig. 1.** Cyclic voltammograms of activated CCDC supercapacitors in the aqueous electrolytes of: (a) 0.5 M $K_2SO_4$, (b) 2 M KCl, (c) 6 M KOH and (d) 1 M $KNO_3$.

Fig. 1 that activated CCDC displays relatively rectangular voltammograms with rapid current responses on voltage reversal at the two end potentials in 2 M KCl (Fig. 1b) and 6 M KOH (Fig. 1c) electrolytes when the scan rates increases from 1 mV $s^{-1}$ to 20 mV $s^{-1}$, which means a good double layer capacitive behavior in above electrolytes. However, for the voltammograms of activated CCDC supercapacitors in the aqueous electrolytes of 0.5 M $K_2SO_4$ (Fig. 1a) and 1 M $KNO_3$ (Fig. 1d), fairly large deformation appear when the scan rates increases from 1 mV $s^{-1}$ to 20 mV $s^{-1}$.

In order to clearly compare the electrochemical behaviors, the CV profiles of activated CCDC supercapacitors in various aqueous electrolytes at a scan rate of 20 mV $s^{-1}$ are displayed in Fig. 2a. All cyclic voltammetric curves of supercapacitors in some electrolyte solutions show analogous shape. However, the curve in 6 M KOH shows relatively constant current response with the change of potential and the current response values is much higher than that of other electrolytes. That is to say, the specific capacitance of the sample in 6 M KOH is the highest among all supercapacitors. The specific capacitance values of all supercapacitors can be determined by Eq. (1): [20]

$$C_{s,t} = \frac{I_a + |I_c|}{2W(dV/dt)} \quad (1)$$

where $C_{s,t}$, $I_a$, $I_c$, $W$ and $dV/dt$ are the specific capacitance (F $g^{-1}$), the current (A) of anodic and cathodic voltammetric curves on positive and negative sweeps, the mass of the material (g) (only including the mass of the activated materials, the same below), and the sweep rate (mV $s^{-1}$), respectively. In a symmetrical two-electrode system, the specific gravimetric capacitance $C_g$ (F $g^{-1}$) for one activated carbon electrode can be obtained from the total capacitance $C_{s,t}$ (F $g^{-1}$) of the cell by the following Eq. (2). [21]

$$C_g = 4C_{s,t} \quad (2)$$

Fig. 2b shows the specific capacitance vs. scan rate. Even at the scan rate of 20 mV $s^{-1}$, the specific capacitance of activated CCDC supercapacitor in the aqueous electrolytes of KOH is 50 F $g^{-1}$, which is higher than others (Zhang et al. [22] studied the electrochemical performances of carbide-derived carbon supercapacitor in 6 M KOH, and the specific capacitance was just 41 F $g^{-1}$ at the scan rate of 20 mV $s^{-1}$). It displays that the specific capacitance of sample in 6 M KOH only decreases by 26% with the scan rate increasing from 1 mV $s^{-1}$ to 20 mV $s^{-1}$. Consequently, the above results demonstrate that the activated CCDC supercapacitor in 6 M KOH performs excellent specific capacitance and good electrochemical reversible behavior.

Theoretically speaking, the differences of the current response and CV behaviors for the supercapacitors in various electrolytes are probably attributed to: (a) the ionic radius of the electrolytes, (b) the radius of ionic hydration sphere of electrolytes, (c) the conductivity of the ions and (d) the mobility of the ions. As well known, the ions should be surrounded by the water of hydration when the water is used as the solvent. It means that the electric double layers will be built by the ionic hydration sphere of electrolytes. The ionic radius of water of hydration, conductivity and ionic mobility of ions are listed in Table 1 [23–25]. It can be seen from Table 1 that the radius of hydration sphere increases in the order: $OH^- < Cl^- < NO^- < SO_4^{2-}$. This order is in good agreement with the CV results, and the radius of water hydration of $OH^-$ ions is 3.00 Å, which is less than other ions so that the size of the water hydration sphere may be a deciding factor on electrochemical properties. Besides, it can be found from Table 1 that the $OH^-$ ions have the higher conductivity and mobility than $NO_3^-$, $SO_4^{2-}$ and $Cl^-$ ions. Therefore, the conductivity and mobility of the ions may be another crucial factor on the supercapacitive performance with different electrolytes.

Compared with the electrolytes of KCl, $KNO_3$, and $K_2SO_4$, the $OH^-$ ion in KOH electrolyte has much higher conductivity of 198 $cm^2\ \Omega\ mol^{-1}$ than $Cl^-$, $NO_3^-$ and $SO_4^{2-}$ ions. Besides, the $OH^-$ ions mobility also shows a higher value of 2.06E−6 $cm^2\ s^{-1}\ v^{-1}$. Hence, the higher conductivity and ionic mobility of $OH^-$ ion can cause much better capacitive behavior. Meanwhile, the higher conductivity

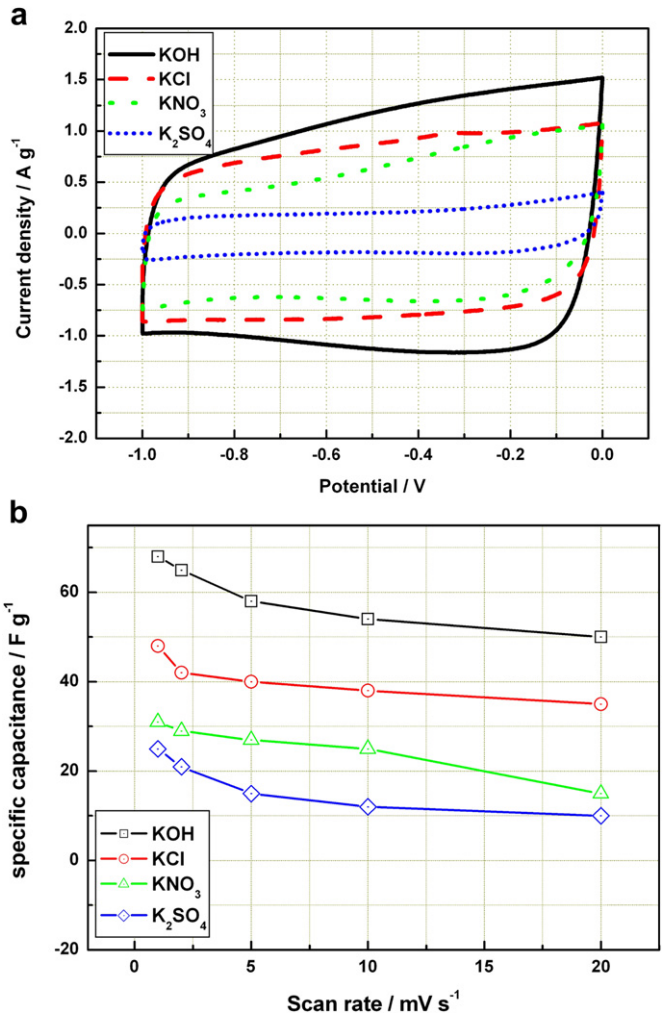


**Fig. 2.** (a) Cyclic voltammograms of activated CCDC supercapacitors in the aqueous electrolytes of 0.5 M $K_2SO_4$, 2 M KCl, 1 M $KNO_3$ and 6 M KOH (20 mV $s^{-1}$), (b) the specific capacitance of the supercapacitor at different scan rates.

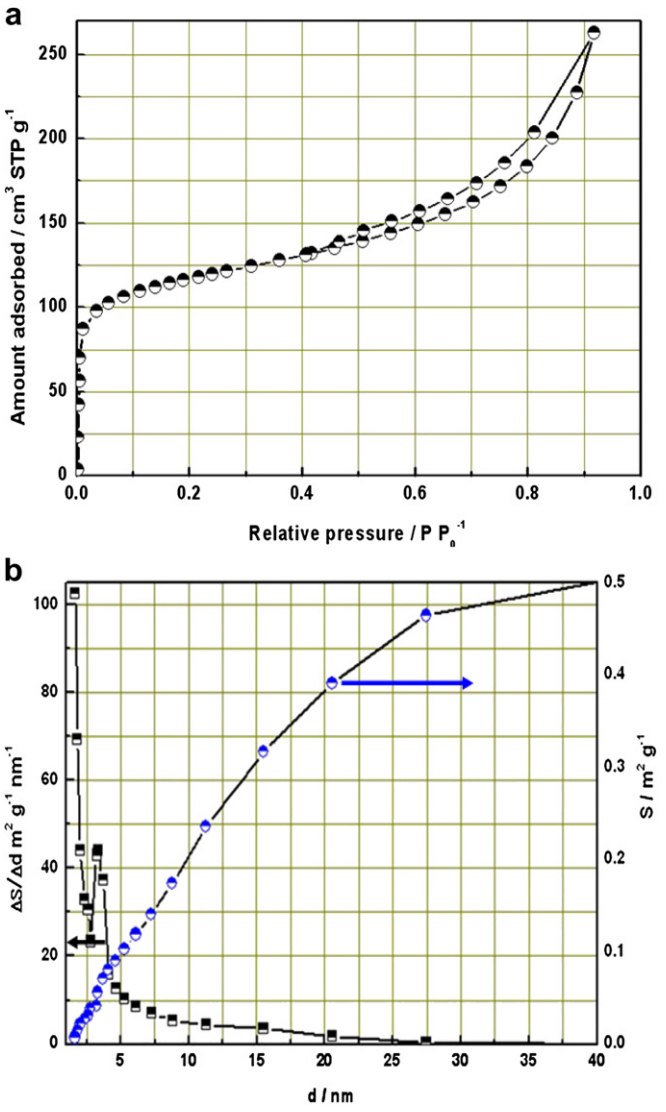


**Fig. 3.** (a) $N_2$ sorption isotherms of carbon samples and (b) Pore size distribution calculated using BJH method.

leads to the higher current response of the CV in KOH than those of the CV in KCl, $KNO_3$ and $K_2SO_4$ electrolytes.

In order to determine the relationship between ions and pore structures, $N_2$ adsorption isotherms are measured to analyze the specific surface area and pore size distribution of activated CCDC. As shown in Fig. 3a, the isotherm of activated CCDC shows a small hysteresis loop at medium relative pressure (type-IV), which is due to the presence of mesopores in the carbon framework. Fig. 3b displays the pore size distribution calculated using BJH method. The pore structure parameters of the activated CCDC samples are all listed in Table 2. It can be found from Table 2 that the $V_{micro}/V_{total}$ is 37%, and the most probable aperture is 0.72 nm. Therefore the activated CCDC has some mesopores besides the large amounts of micropores. The schematic diagram of the relationship of hydration sphere ions and pores is shown in Fig. 4. In the KCl, $KNO_3$ and KOH electrolytes, the radii of hydration sphere of $Cl^-$ and $NO_3^-$ ions are just slightly higher than the $OH^-$ ion, and the most probable apertures are equal to about 2.1× the size of the radii of hydration spheres (Fig. 4a). But for the $K_2SO_4$ electrolyte, the radius of hydration sphere of $SO_4^{2-}$ ion is the biggest of all (the most probable aperture is just equal to about 1.8× the size of the radius of hydration sphere (Fig. 4b)), leading to a decrease in quantity of ions entering into pores, thus lower electric double layer is formed [26]. Furthermore, the conductivity and ionic mobility of $SO_4^{2-}$ ion are at relatively low level. Therefore, the activated CCDC supercapacitor in the 0.5 M $K_2SO_4$ aqueous electrolyte performs a poor capacitive behavior. In brief, even at higher scan rates, the activated CCDC supercapacitor in the aqueous electrolyte of 6 M KOH performs excellent capacitive behavior due to excellent properties of $OH^-$ ions.

**Table 1**
Radius of hydration sphere, conductivity and ionic mobility of ions.

| Items | Ion | | | |
|---|---|---|---|---|
| | $OH^-$ | $Cl^-$ | $NO_3^-$ | $SO_4^{2-}$ |
| Radius of hydration sphere (Å) | 3.00 | 3.32 | 3.35 | 3.79 |
| Conductivity ($cm^2\ \Omega\ mol^{-1}$) | 198.00 | 76.34 | 71.44 | 79.80 |
| Ionic mobility ($\mu\ 10^{-5}\ cm^2\ s^{-1}\ v^{-1}$) | 20.60 | 7.91 | 7.40 | 8.30 |

**Table 2**
Pore structure parameters of activated CCDC.

| Samples | Surface area ($m^2\ g^{-1}$) | | Most probable aperture (nm) | Volume ($cm^3\ g^{-1}$) | |
|---|---|---|---|---|---|
| | $S_{BET}$ | $S_{micro}$ | | $V_{total}$ | $V_{micro}$ |
| Activated CCDC | 437 | 153 | 0.72 | 0.81 | 0.30 |

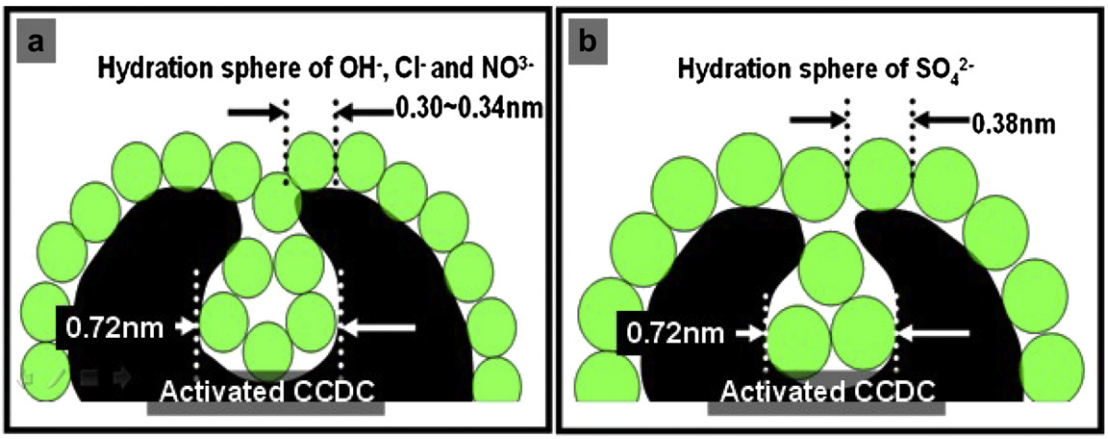


**Fig. 4.** Schematic diagram of the relationship of hydration sphere ions and pores.

Fig. 5 presents the charge/discharge curves of activated CCDC supercapacitors (between 0 V and 1 V) measured at the current densities of 0.5 A $g^{-1}$ in 0.5 M $K_2SO_4$, 2 M KCl, 1 M $KNO_3$ and 6 M KOH, respectively. The curves of the activated CCDC supercapacitors in 2 M KCl and 6 M KOH are almost symmetrical isosceles lines, demonstrating that the activated CCDC supercapacitors have typical porous carbon supercapacitive behavior and stable electrochemical properties in above electrolytes [27]. Furthermore, the curve of the activated CCDC supercapacitors in 6 M KOH shows longer discharge time than other electrolytes, which means that it possesses higher specific capacitance value in 6 M KOH at current densities of 0.5 A $g^{-1}$. This is in good agreement with the CV results. Particularly, at the beginning of discharge there are a few sudden potential drop (IR drop), which are attributed to the ohmic resistance of electrolytes and the inner resistance of ion diffusion in micropore. Usually, IR drop is a direct measure of equivalent series resistance (ESR) which influences the overall power performance of a capacitor. The inset in Fig. 5 depicts the IR drops of activated CCDC supercapacitors in 2 M KCl and 6 M KOH to clearly compare the IR value. It can be found that the IR drop for the activated CCDC supercapacitors in 6 M KOH is less than that in 2 M KCl.

The specific capacitances of supercapacitors can be calculated by Eq. (3) [28]

$$C_m = \frac{itd}{m\Delta V} \tag{3}$$

Here, $C_m$ is the specific capacitance (F $g^{-1}$), $i$ is the charge/discharge current (A), $\triangle V$ is the potential range of the charge/discharge (V), $t_d$ is the discharge time (s), and $m$ is the mass of active material (g) within the electrode.

The specific capacitance of the activated CCDC supercapacitors vs. current density and electrolyte are shown in Fig. 6. It further demonstrates the dependence of the specific capacitance values (evaluated by Eq. (3)) on current density (from 0.5 A $g^{-1}$ to 2 A $g^{-1}$) and electrolyte (0.5 M $K_2SO_4$, 2 M KCl, 1 M $KNO_3$ and 6 M KOH) for all the supercapacitors. The specific capacitance value of activated CCDC supercapacitors in the aqueous electrolytes of 6 M KOH is much higher than that of other electrolytes. It also can be noted that even at higher current density of 2 A $g^{-1}$, the specific capacitance of activated CCDC still maintains retention of more than 80% in 6 M KOH. Consequently, the results obtained from galvanostatic charge/discharge show that the activated CCDC supercapacitor in 6 M KOH electrolyte performs excellent electrochemical reversible behavior, outstanding rate capability and lower IR drop.

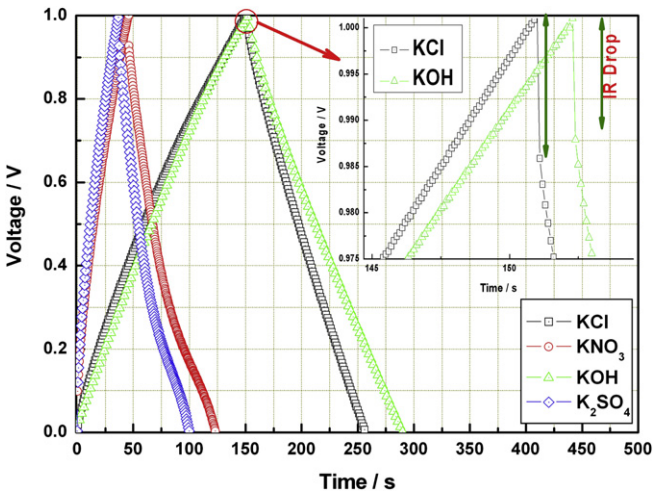


**Fig. 5.** The galvanostatic charging/discharging curves of the activated CCDC supercapacitors at the current densities of 0.5 A $g^{-1}$ in 0.5 M $K_2SO_4$, 2 M KCl, 1 M $KNO_3$ and 6 M KOH (IR drop of activated CCDC supercapacitors in 2 M KCl and 6 M KOH inset).

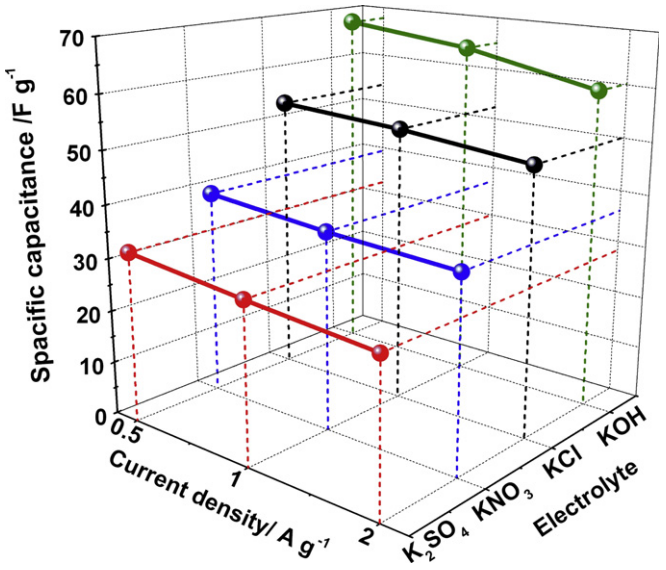


**Fig. 6.** The specific capacitance (*Z*-axis) of the activated CCDC supercapacitors vs. current density (*X*-axis) and electrolyte (*Y*-axis).

The Ragone plots (Fig. 7) are frequently used in demonstration of power densities and energy densities of supercapacitors. The energy density (Wh $kg^{-1}$) is calculated by Eq. (4): [29]

$$E = \frac{1}{2} C_m V^2 \quad (4)$$

where $C_m$ is the specific capacitance of the two-electrode capacitor (F $g^{-1}$), $V$ is the voltage decrease in discharge (V). The power density (W $kg^{-1}$) is calculated by Eq. (5): [29]

$$P = \frac{2E}{\Delta t_d} \quad (5)$$

where $E$ is the energy density (Wh $kg^{-1}$), $\Delta t_d$ is the time spent in discharge (s). As shown in Fig. 7, the energy densities of all activated CCDC in 6 M KOH electrolyte are obviously better than those in other electrolytes. The highest energy densities can be obtained from 6 M KOH. As the power density increases from 498 W $kg^{-1}$ to 1992 W $kg^{-1}$, the energy density drops from 9.4 Wh $kg^{-1}$ to 8.3 Wh $kg^{-1}$ and the other lines show similar trends. The energy and power limitations normally observed at high rates are associated with the complex resistance and the tortuous diffusion pathways within the porous textures. The good energy and power performances of activated CCDC in 6 M KOH confirm that micropores and mesoporous of activated CCDC can be effectively utilized for charge storage [30]. Therefore, the 6 M KOH solution is more promising electrolyte for the applications of supercapacitor using activated CCDC as electrode active material, where high power outputs as well as high energy capacities are required, such as in electric vehicles.

Electrochemical impedance spectroscopy (EIS) is measured to analyze the electrochemical properties of supercapacitors about characteristic frequency responses. Fig. 8a shows the ac impedance spectrum (Nyquist plots) for activated CCDC supercapacitors in 0.5 M $K_2SO_4$, 2 M KCl, 1 M $KNO_3$ and 6 M KOH, respectively. It can be found in Fig. 8a that there are straight lines in the low-frequency region (lower than 100 Hz) because of Warburg impedance [31]. The straight line part leans more towards the imaginary axis, thus indicating a good capacitive behavior. The deviations from the vertical lines are ascribed to the inner mesopore diffusion, which is strongly dependent on the measured potentials. Furthermore, the impedance in high frequency has a special arc-shaped curve that means the microstructures of orbicular pores [32]. In most cases,

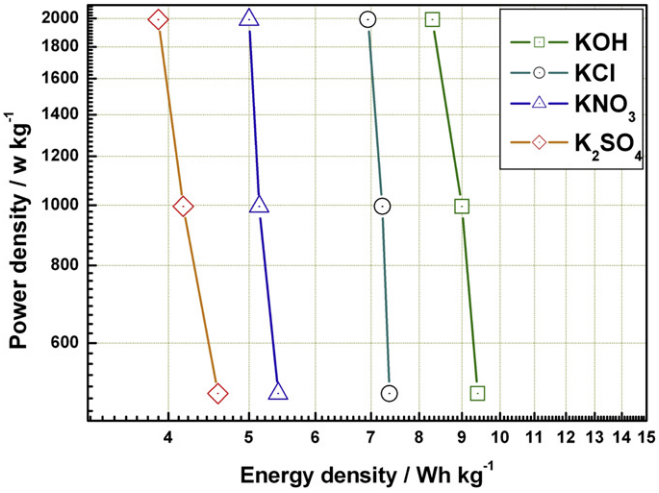


**Fig. 7.** Ragone plots for activated CCDC supercapacitors.

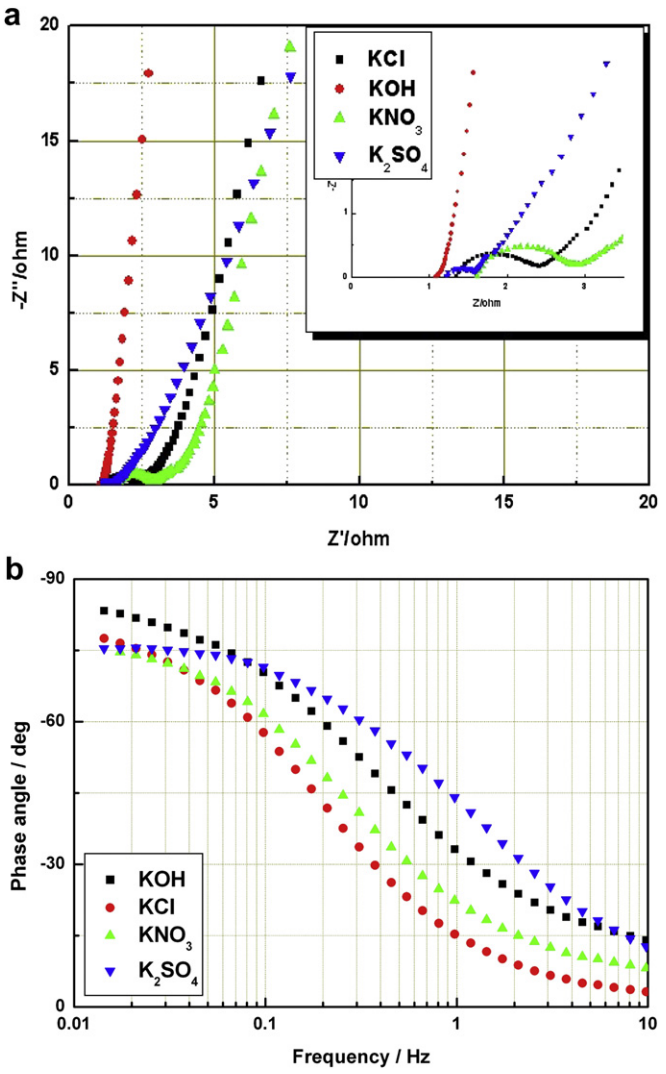


**Fig. 8.** (a) Nyquist plot based on activated CCDC electrodes with the frequency range of $10^5$ Hz–$10^{-2}$ Hz (the inset shows the expanded high-frequency region of the plot) and (b) Bode phase angle plots vs. frequency dependencies of the activated CCDC supercapacitors in different electrolytes.

the depressed semicircles are considered as small charge-transfer resistances between the electrode and the electrolytes. Here, charge-transfer resistance is extremely low from the inconspicuous semicircle for the activated CCDC in KOH electrolyte (Fig. 8a inset). Since the diameters of the semicircles decrease in the order of $KNO_3 > KCl > K_2SO_4 > KOH$, it is speculated that the semicircles are also associated with the different ionic dynamic dispersion within the pores, and the mobility of hydrated ions in the inner pores increase in the order of $NO_3^- < Cl^- < SO_4^{2-} < OH^-$. In addition, as being seen from the intercept with real axis at high frequency, the resistance of bulk electrolyte decreases in the order of $KNO_3 > KCl > K_2SO_4 > KOH$, which verifies the conductivity sequence of $NO_3^- < Cl^- < SO_4^{2-} < OH^-$ (Table 1).

The Bode plots for the activated CCDC supercapacitors in different electrolytes are shown in Fig. 8b. As being seen in Fig. 8b, the response time is above −75° phase, and it can be found that the supercapacitor in 6 M KOH electrolyte gives the fastest response time. This result suggests that the charge-storage contribution of supercapacitor in 6 M KOH become fast as an increase in frequency. Moreover, the phase angle is close to −80° (the ideal one should be −90°) at lower frequency limitation,

further proving the good capacitive property of the supercapacitor in 6 M KOH electrolyte.

The supercapacitors behave as a series combination of a resistance and capacitance and both of them depend on the frequency in EIS measure. In the low-frequency region, the capacitance ($C(\omega)$) can be defined as the combination of real part of the capacitance ($C'(\omega)$) and imaginary of the capacitance ($C''(\omega)$), and they can be calculated as following Eqs. (6) and (8): [33]

$$C(\omega) = C'(\omega) + jC''(\omega) \tag{6}$$

$$C'(\omega) = -\frac{Z''(\omega)}{\omega|Z(\omega)|^2} \tag{7}$$

$$C''(\omega) = \frac{Z'(\omega)}{\omega|Z(\omega)|^2} \tag{8}$$

Here $C'(\omega)$ corresponds to the static capacitance which is tested during the constant current discharge, $C''(\omega)$ corresponds to energy dissipation of the supercapacitor by IR drop and an irreversible faradic charge-transfer process, which can cause the hysteresis of the electrochemical processes. $|Z(\omega)|$ is the impedance modulus, and $\omega$ is the angular frequency. Moreover, the $C''(\omega)$ versus frequency ($f$) dependence has a maximum at the so-called relaxation frequency $f_R$, determining the characteristic time constant RC called relaxation time $\tau_R$. $\tau_R$ is a quantitative measure of how fast the device can be charged and discharged reversibly, and it can be calculated by Eq. (9): [34]

$$\tau_R = (2\pi f_R)^{-1} \tag{9}$$

Fig. 9 shows the comparison of $C''(\omega)$ vs. $f$ plots for activated CCDC supercapacitors in different electrolytes and the values of $\tau_R$ of the supercapacitors in different electrolytes were calculated and indicated in Fig. 9. It proves that $\tau_R$ depends strongly on the electrolyte characteristics. However, $\tau_R$ of the activated CCDC supercapacitor in 6 M KOH is the least because of the fast mobility of $OH^-$ ions. The values of $\tau_R$ of the supercapacitors in different electrolytes increase in the order: KOH < $K_2SO_4$ < KCl < $KNO_3$, which is in good agreement with the ionic mobility listed in Table 1. Therefore, the KOH-based

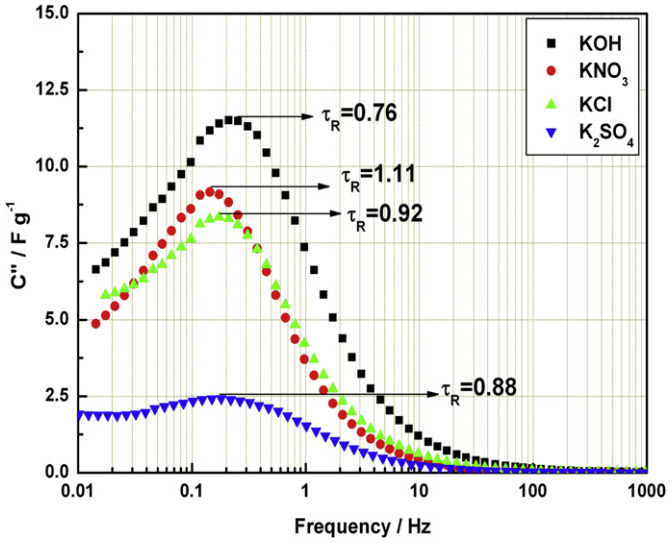


**Fig. 9.** The Imaginary capacitance vs. frequency dependencies of the supercapacitors in different electrolytes.

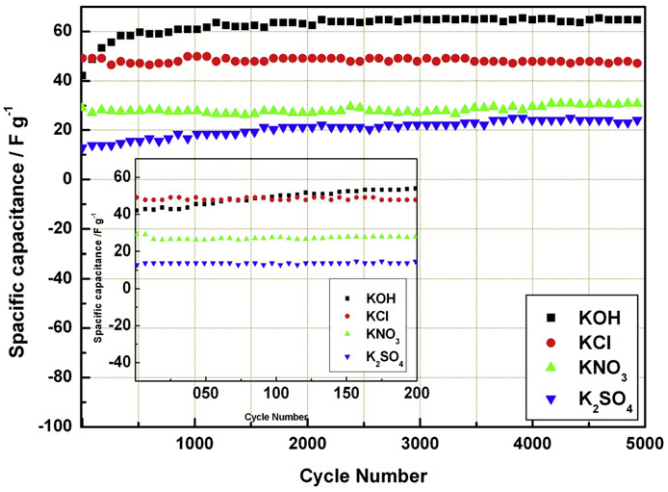


**Fig. 10.** The cycle life curve of activated CCDC supercapacitors in the aqueous electrolytes of $K_2SO_4$, KCl, $KNO_3$ and KOH at current density of 1 A $g^{-1}$.

electrolyte shows much better rate performance than others, which is consistent with the results from Fig. 2b.

The long cycle life is one of the most important properties for appliances of supercapacitors. The specific capacitances versus cycle number with constant current charge/discharge cycle at the voltage range from 0 V to 1 V for all supercapacitors are shown in Fig. 10. It reveals the change of specific capacitance versus cycle number for activated CCDC supercapacitors in various electrolytes at the constant current charge/discharge density of 1 A $g^{-1}$. After 5000 consecutive cycles, the specific capacitances still keep at 68, 52, 31 and 25 F $g^{-1}$ for the activated CCDC in 6 M KOH, 2 M KCl, 1 M $KNO_3$ and 0.5 M $K_2SO_4$, respectively. Besides, there are up trends in the cycle curves of the activated CCDC in 6 M KOH at the beginning cycles (Fig. 10 inset), maybe it needs more time in initial several charging/discharging cycles to let the electrolyte completely enter into the pores of the electrode material [35]. These data illustrate further that the supercapacitors using the activated CCDC as electrode active materials present good cycling stability in the repetitive charge/discharge cycling. Particularly, the supercapacitor using 6 M KOH as electrolyte exhibits excellent cyclic stability and higher specific capacitances.

## 4. Conclusion

Cyclic voltammetry, galvanostatic charge/discharge, electrochemical impedance spectroscopy and cyclic life have been used to compare the electrochemical behaviors for the supercapacitors based on the activated CCDC electrode material in 0.5 M $K_2SO_4$, 2 M KCl, 1 M $KNO_3$ or 6 M KOH electrolyte solutions, respectively. The activated CCDC supercapacitor in 6 M KOH has electrochemical capacitance of 68 F $g^{-1}$ at the scan rate of 1 mV $s^{-1}$ within potential window 0 V–1 V. It delivers an energy density of 8.3 Wh $kg^{-1}$ and a power density of 1992 W $kg^{-1}$ based on the total weight of the electrode active materials as well as excellent electrochemical reversible behavior, outstanding rate capability and lower IR drop. Moreover, the phase angle of the supercapacitor in 6 M KOH electrolyte is close to −80° (the ideal one should be −90°) at lower frequency limitation and the relaxation time is as low as 0.76 s because of the fast mobility of $OH^-$ ions. The supercapacitor also exhibits a good cycling performance and keeps 95% of initial capacity over 5000 cycles. Therefore, 6 M KOH solution is a more promising electrolyte for the application of supercapacitor using activated CCDC as electrode active material.

## Acknowledgements

This work was financially supported by the National Natural Science Foundation of China (Grant Nos. 51272221, 51072173 and 21203161), Specialized Research Fund for the Doctoral Program of Higher Education (Grant No. 20094301110005), the Scientific Research Fund of Hunan Provincial Education (Grant No. 11C1210).

## References

[1] E. Frackowiak, F. Béguin, Carbon 39 (2001) 937–950.
[2] A. Burke, J. Power Sources 91 (2000) 37–50.
[3] T. Xue, C.L. Xu, D.D. Zhao, X.H. Li, H.L. Li, J. Power Sources 164 (2007) 953–958.
[4] P. Liu, M. Verbrugge, S. Soukiazian, J. Power Sources 156 (2006) 712–718.
[5] B. Xu, F. Wu, R.J. Chen, G.P. Cao, S. Chen, G.Q. Wang, Y.S. Yang, J. Power Sources 158 (2006) 773–778.
[6] H.T. Liu, G.Y. Zhu, J. Power Sources 171 (2007) 1054–1067.
[7] J.P. Zheng, T.R. Jow, J. Electrochem. Soc. 144 (1997) 2417–2420.
[8] C.M. Yang, Y.J. Kim, M. Endo, H. Kanoh, M. Yudasaka, S. Iijima, K. Kaneko, J. Am. Chem. Soc. 129 (2007) 20–21.
[9] K.C. Tsay, L. Zhang, J.J. Zhang, Electrochim. Acta 60 (2012) 428–436.
[10] H.Y. Lee, J.B. Goodenough, J. Solid State Chem. 144 (1999) 220–223.
[11] Y.J. Hao, Q.Y. Lai, L. Wang, X.Y. Xu, H.Y. Chu, Synth. Met. 160 (2010) 669–674.
[12] L.P. Zheng, Y. Wang, X.Y. Wang, X.Y. Wang, H.F. An, L.H. Yi, J. Mater. Sci. 45 (2010) 6030–6037.
[13] G. Yushin, R. Dash, J. Jagiello, J.E. Fischer, Y. Gogotsi, Adv. Funct. Mater. 16 (2006) 2288–2293.
[14] M. Schmirler, F. Glenk, J.M. Etzold Bastian, Carbon 49 (2011) 3679–3686.
[15] C.L. Dai, X.Y. Wang, Y. Wang, N. Li, J.L. Wei, Mater. Chem. Phys. 112 (2008) 461–465.
[16] L.P. Zheng, Y. Wang, X.Y. Wang, N. Li, H.F. An, H.J. Chen, J. G, J. Power Sources 195 (2010) 1747–1752.
[17] H. Wu, X.Y. Wang, X.Y. Wang, X.Y. Zhang, L.L. Jiang, B.A. Hu, L.P. Wang, J. Solid State Electrochem. (2012). http://dx.doi.org/10.1007/s10008-012-1726-3.
[18] T.E. Rufford, D. Hulicova-Jurcakova, K. Khosla, Z.H. Zhu, G.Q. Lu, J. Power Sources 195 (2010) 912–918.
[19] J. Yang, K.Q. Qiu, Environ. Sci. Technol. 43 (2009) 3385–3390.
[20] C.C. Hu, C.C. Wang, Electrochem. Commun. 4 (2002) 554–559.
[21] A. .Jänes, H. .Kurig, E. Lust, Carbon 45 (2007) 1226–1233.
[22] X.Y. Zhang, X.Y. Wang, L.L. Jiang, H. Wu, C. Wu, J.C. Su, J. Power Sources 216 (2012) 290–296.
[23] R.D. Shannon, Acta Cryst. A32 (1976) 751–767.
[24] R.S. Berry, S.A. Rice, J. Ross, Physical Chemistry, Wiley, 1980.
[25] B. Tansel, J. Sager, T. Rector, J. Garland, R.F. Strayer, L. Levine, M. Roberts, M. Hummerick, J. Bauer, Sep. Purif. Technol. 51 (2006) 40–47.
[26] C.R. Pérez, S.H. Yeon, J. Ségalini, V. Presser, P.L. Taberna, P. Simon, Y. Gogotsi, Adv. Funct. Mater. (2012). http://dx.doi.org/10.1002/adfm.201200695.
[27] S. Mitani, S.I. Lee, K. Saito, Y. Korai, I. Mochida, Electrochim. Acta 51 (2006) 5487–5493.
[28] Y.G. Wang, H.Q. Li, Y.Y. Xia, Adv. Mater. 18 (2006) 2619–2623.
[29] W.G. Pell, B.E. Conway, J. Power Sources 63 (1996) 255–266.
[30] W.H. Jin, G.T. Cao, J.Y. Sun, J. Power Sources 175 (2008) 686–691.
[31] X.Y. Zhang, X.Y. Wang, J.C. Su, X.Y. Wang, L.L. Jiang, H. Wu, C. Wu, J. Power Sources 199 (2012) 402–408.
[32] H. Keiser, K.D. Beccu, M.A. Gutjahr, Electrochim. Acta 21 (1976) 539–543.
[33] J. Eskusson, A. Jänes, A. Kikas, L. Matisen, E. Lust, J. Power Sources 196 (2011) 4109–4116.
[34] D. Wang, W. Ni, H. Pang, Q. Lu, Z. Huang, J. Zhao, Electrochim. Acta 55 (2010) 6830–6835.
[35] W.C. Chen, T.C. Wen, H. Teng, Electrochim. Acta 48 (2003) 641–649.